Macromolecules

Article

pubs.acs.org/Macromolecules

Effect of Solution Parameters on Spontaneous Jet Formation and Throughput in Edge Electrospinning from a Fluid-Filled Bowl

Nagarajan M. Thoppey,[†] Russell E. Gorga,[†] Jason R. Bochinski,[‡] and Laura I. Clarke*[,‡]

[†]Fiber and Polymer Science Program, North Carolina State University, Raleigh, North Carolina 27695, United States

[‡]Department of Physics, North Carolina State University, Raleigh, North Carolina 27695, United States

ABSTRACT: The process of edge electrospinning relies on forming electric-field-induced instabilities (i.e., jets) in a polymer solution bath which act as sources for nanofiber production. As such, it depends on the fundamental interactions between the fluid and the electric field, which are studied in this report as a function of solution parameters (viscosity, surface tension, and conductivity). Over a wide range of conditions, experimental observations including time required for initial jet formation, total number of jets, feed rate per jet, and resultant fiber diameter are reported and compared with theoretical predictions. The presently realized fiber throughput is 40× a single needle approach while maintaining similar high fiber quality. Two distinct voltage intervals are utilized to generate many fiber-forming instabilities: a high level for jet creation and then reduced amplitude for fiber production. This dual-stage approach relies on hysteresis in Taylor cone-jet formation, wherein a larger voltage is required to create a jet-emitting cone than to maintain it.

1. INTRODUCTION

Study and development of nanofibrous materials have dramatically increased over the past 15 years. Such scholarly activities still continue at a torrid pace today, driven by the technologically useful properties possessed by collections of nanofibers, including high surface-area-to-volume ratios,[1−5] high porosity,[6−9] and morphological biocompatibility.[7−24] At the research-level production scale, the most widely used technique for nanofiber fabrication is electrospinning,[25−32] which utilizes an electric field to "draw" a polymer fluid into a fiber. Thus, the technology of electrospinning implicitly relies on fundamental understanding of the interaction between a charged fluid and an applied electric field. For instance, under the common traditional needle electrospinning (TNE) approach, where polymer solution is mechanically pumped through a fine conducting needle placed at high voltage, the electric field forms a Taylor cone at the needle tip, providing an electrostatic suction which combines with the pump-controlled feed rate to propel the fluid. The fluid jet emanating from the Taylor cone initially moves along a linear path for a short distance (in the region near to the needle), until the still-forming, charged fiber develops a whipping instability (relatively far from the needle), resulting in dramatic fiber elongation and narrowing, before subsequently depositing onto an electrically grounded collector (Figure 1a).[29] New variations to the TNE approach continue to appear on a regular basis.[33−35]

A fundamental limitation of nanofiber formation using the TNE configuration is that the overall production rate is low (0.01−0.1 g/h[36,37]), which impedes industrial scale implementation; thus, methodologies that demonstrate higher fabrication rates are desirable. Recently, we have developed an alternative electrospinning approach[38,39] where, instead of physically pumping fluid through a needle, the electric field itself is tuned to generate fluid instabilities within a bath reservoir comprised of a thin-lipped bowl filled with polymer solution (Figure 1b). Such fluid perturbations are akin to the Rayleigh−Taylor instabilities[40] formed by gravity forces in a thin film, e.g., when a layer of wet paint on a ceiling spontaneously breaks into a series of droplets with a distinctive spacing that is determined by the fluid properties and the strength of the perturbing force. Here, such electric-field-induced fluid instabilities produce jet-emitting Taylor cones similar to those found at the needle tip in TNE. In general, such unconfined electrospinning approaches (where the fluid is not directed through a physically restricting nozzle) allow a multitude of jets to spontaneously form and reorganize efficiently, providing for many simultaneous jets without additional engineering design complexity (for instance, in a configuration of an array of many needles). The fluid properties and the electric field intensity and history determine the number of stable jets and feed rate per jet (rather than being dominantly controlled by the directed mechanical pumping as in TNE). In bowl-edge electrospinning, the symmetry of the experimental apparatus (combining the metal bowl held at high voltage as a source electrode with a grounded cylindrical collector) permits many jets to be formed along the lip of the bowl and efficiently organize into a symmetrically spaced arrangement, partially minimizing jet-to-jet interactions as the distance between neighboring jets increases with radial distance in this concentric geometry. In

Received: June 14, 2012
Revised: July 17, 2012
Published: July 30, 2012

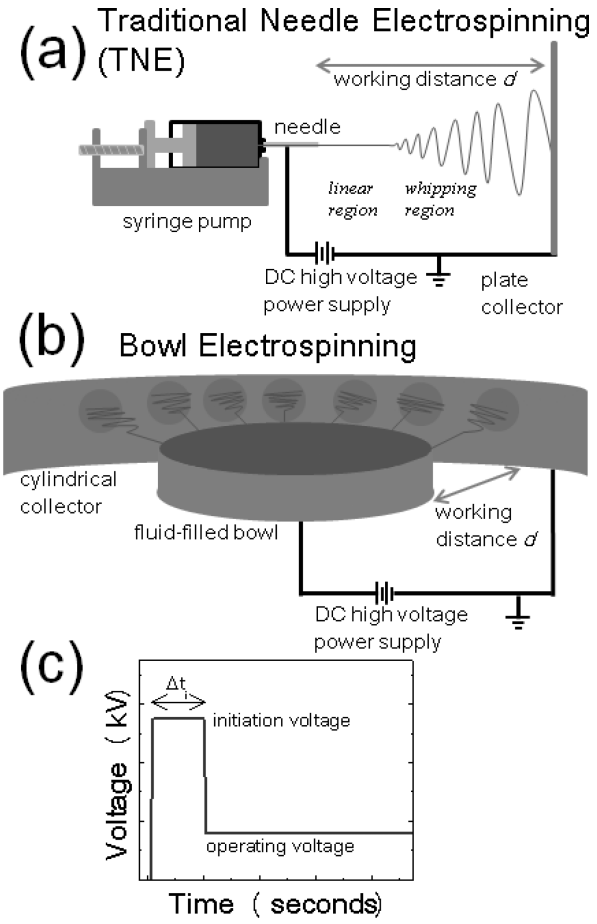

Figure 1. (a) A traditional needle electrospinning (TNE) apparatus consisting of a precision syringe pump, conducting needle, dc high-voltage power supply, and grounded plate collector. (b) Bowl electrospinning schematic comprising a thin-lipped, stationary fluid-filled bowl, dc high-voltage power supply, and concentric grounded collector. Note: for ease of viewing, the collector is not fully depicted. (c) For hysteretic electrospinning, a high-amplitude initiation voltage is applied for a brief time interval (Δt_i), before rapidly reduced to lower, operating voltage level.

addition, because the electric field can be tuned to provide an effective feed rate per jet, similar to that present in needle electrospinning, throughput from this simple system can be dramatically higher than in TNE (40× higher for a single filling of the bowl) while maintaining high nanofiber quality. Other unconfined electrospinning approaches that have been demonstrated include cleft electrospinning where jets are formed in a rectangular bath and spin upward to a flat collector,[41] needleless electrospinning from a fluid-coated sphere,[42] and the commercial instrument Nanospider.[43] We note reviews of some electrospinning schemes for scaling-up nanofiber production rates have appeared recently.[44,45]

In the bowl-edge unconfined electrospinning approach, the fundamental interaction between the electric field and the polymer solution is now responsible for developing fluid perturbations, determining the feed rate, and providing sufficient jet charge and an appropriate electric field distribution to maintain a similar pattern of linear motion and whipping as in TNE (in order to ensure that that fiber quality is equivalent to that produced by the standard technique). In this work, we explore the various aspects of this underlying interaction by systematically modifying the fluid properties (solution concentration, viscosity, surface tension, and conductivity) and observe the resultant changes in jet number, mass throughput per jet, and resultant fiber morphology in this unconventional bowl-based approach. Utilizing simple models to explain these results, we discuss how fundamental understanding of the fluid−field interaction can be used to maximize the number of available spinning sites (jets) in a given configuration while still maintaining high fiber quality. Comparing the experimental results with existing theoretical models of electrically induced instability formation,[42] the observed relative time for jet formation and jet density match well with predictions, except when jet-to-jet interactions are strong (i.e., under conditions of very high jet density). By using such a model, the advantages of a two-stage voltage process, where a high voltage level is first utilized to initiate jets and then a lower voltage is applied at which jets can be maintained but not created (i.e., the jet creation rate under the lower voltage condition is impractically slow), are clearly delineated. To our knowledge this is the first time that the property of hysteresis in Taylor cone-jet formation[46−49]—i.e., where a higher voltage creates a cone jet and a lower voltage sustains it—has been explicitly utilized to facilitate the scale-up of nanofiber production rate.

Thus, bowl-edge electrospinning experiments provide an exemplary system in which the physics underlying fluid−electric field interactions can be studied. We discuss the connection between fundamental fluid fluctuation length scales and the experimental results, addressing the complex relation-

Table 1. Properties of PEO Electrospinning Solutions as a Function of Polymer, Salt, and Surfactant Concentrations[a]

solution no.	PEO concn (wt %)	concn (wt %) or (v/v)	zero shear viscosity (cP)	conductivity (μS/cm)	surface tension (mN/m)
1	4		1050 ± 50	83.8 ± 0.5	61.9 ± 0.3
2	5		2900 ± 150	84.2 ± 0.7	61.4 ± 0.4
3	6		7480 ± 370	84.7 ± 0.2	59.6 ± 0.4
4	7		17080 ± 850	86.7 ± 0.6	57.7 ± 0.3
5	6	0.001 NaCl	7470 ± 370	108.2 ± 0.4	61.8 ± 0.1
6	6	0.005 NaCl	7470 ± 370	182.5 ± 0.5	61.7 ± 0.1
7	6	0.01 NaCl	7460 ± 370	255.7 ± 8.6	60.0 ± 0.3
8	6	0.05 NaCl	7440 ± 370	905.3 ± 13.4	60.2 ± 0.2
9	4	0.1 Triton	1085 ± 54	131.3 ± 0.5	31.1 ± 0.1
10	6	0.1 Triton	7460 ± 370	100.7 ± 0.7	32.4 ± 0.4
11	7	0.1 Triton	17530 ± 880	104.0 ± 0.5	31.2 ± 0.9
12	7	0.001 NaCl	17030 ± 850	113.2 ± 0.4	57.2 ± 0.4

[a]To all solutions, 0.001 wt % R6G was also added to aid imaging contrast.

dx.doi.org/10.1021/ma301207t | Macromolecules 2012, 45, 6527−6537

ships resulting from the combination of cohesive fluid forces, forces exerted by the electric field on the charged fluid, and jet-to-jet forces due to electrostatic repulsion.

2. EXPERIMENTAL SECTION

2.1. Materials. Poly(ethylene oxide) (PEO) with an average molecular weight of 400 000 g/mol (Scientific Polymer Products), an inorganic salt sodium chloride (NaCl, crystalline/certified ACS) (Fisher Scientific), a nonionic surfactant Triton X-100 (Triton, T9284, 625 g/mol) (Sigma-Aldrich), and a dye molecule Rhodamine 590 Chloride (R6G, 05901, 479 g/mol) (Exciton) were purchased. Deionized water was used as the solvent, and all materials were used without further purification.

Polymer solutions were prepared at various concentrations of PEO, NaCl, and Triton, in order to obtain a wide range of solution properties[50,51] (e.g., viscosity, conductivity, and surface tension). The concentrations of PEO, NaCl, and Triton were carefully selected such that one specific solution property was intentionally varied while maintaining the others at a comparably fixed level. For example, in order to obtain a range of fluid viscosities without altering conductivity or surface tension, solutions of 4, 5, 6, and 7 wt % PEO in deionized water were used. For the generation of varying solution conductivities with minimal change in surface tension or viscosity, solutions were prepared consisting of 0.001, 0.005, 0.01, 0.05, and 0.1 wt % NaCl (salt:water) in 6 wt % PEO in deionized water; in addition, a 0.001 wt % NaCl in 7 wt % PEO solution was also tested. The amount of the liquid surfactant utilized in the solutions is quantified as the percentage of surfactant volume to water volume (v/v) used in the solution; in order to generate fluids possessing reduced surface tension, solutions were prepared of 0.1% Triton v/v in 4, 6, and 7 wt % PEO solutions. Because the surfactant also slightly raised the solution conductivity, these results were compared with pure PEO solutions with a small addition of salt (0.001 wt %). The viscosity of the solutions was unchanged with the presence of the surfactant. In addition, solutions often contained a trace amount (0.001 wt %) of R6G to provide optical contrast for enhanced viewing. Table 1 summarizes the measured properties of the 12 solutions predominantly utilized in this work. All solutions were stirred at room temperature for 24 h to aid dissolution.

2.2. Solution Characterization. The zero shear viscosity of the different solutions was measured with a stress-controlled rheometer (REOLOGICA Instruments AB, StressTech) having a parallel plate geometry (45 mm diameter and a plate gap of 0.4 mm). Solution conductivities were determined utilizing a portable waterproof conductivity meter (Fisher Scientific, Accumet AP85) with a plastic-bodied probe. The surface tension of each solution was evaluated using the Wilhelmy-plate method by a surface tensiometer (Future Digital Scientific Corp., DCAT11). All measurements took place at 25 °C.

2.3. Apparatus. Figure 1a shows a schematic representation of the traditional needle electrospinning (TNE) setup utilized for control experiments. The apparatus consisted of a 10 mL plastic syringe, a programmable syringe pump (New Era Systems, Model # NE-1000), a 10 cm long, blunt tip, gauge 20, stainless steel needle (Sigma-Aldrich) electrically connected to a positive polarity, high-voltage power supply (Glassman High Voltage, Model # FC60R2), and a circular aluminum collector plate (15.25 cm in diameter and 0.3 cm thickness) connected to ground potential. The collector plate was located a working distance d from the needle tip, centered on and oriented orthogonally to the needle's long axis; electrospinning occurred in the horizontal direction. Polymer solution was supplied through the needle at a controlled feed rate using the syringe pump. The optimized parameters for the production of high-quality nanofibers using a 6 wt % PEO solution were an applied voltage of 11 kV, a working distance of 15 cm, and a solution feed rate of 5 μL/min. These parameters were fixed for all TNE experiments, except where otherwise explicitly noted.

Figure 1b shows a schematic representation of the bowl electrospinning experimental apparatus. The cylinder-shaped aluminum bowl (machined from a single solid piece to dimensions of 9 cm inside diameter, 0.03 cm wall thickness, and 0.9 cm depth) was electrically connected to the positive polarity output of a high-voltage power supply, and an aluminum concentric, hollow cylinder (39 cm in diameter, 0.01 cm in thickness, and 38 cm in height and electrically connected to ground potential) acted as the collector. The working distance d, between the outer surface of the bowl and the inner surface of the collector, was fixed at 15 cm. The cylindrical collector could be smoothly translated vertically along the direction of the center axis of the bowl while maintaining a constant working distance; at all times the collector extended at least ±9 cm relative to the horizontal plane defined by the upper bowl lip. A fixed initial volume of polymer solution (78 mL) was loaded into the bowl before each experiment. A circular drain port, located in the center of the bowl, was sealed with a 1.27 cm diameter plastic plug. In both TNE and bowl electrospinning experiments, the collector surfaces that faced the source electrodes (needle or bowl) were completely covered with conductive aluminum foil (Home 360, 16 ± 1 μm in thickness) in order to easily remove the electrospun mat samples for analysis.

As depicted in Figure 1c, bowl electrospinning experiments utilized two different voltages, referred to as "initiation" and "working" or "operating". Each experiment began by application of a high-voltage level (the initiation voltage) for a brief time period (Δt_i). The purpose of the initiation interval is to quickly form many jets and allow these jets to self-organize and stabilize near the edge of the bowl. During the initiation period, multiple fluid instabilities formed spontaneously on the polymer solution surface and electrospraying or streaming events occurred (i.e., wet solution was propelled directly to the collector); thus, fiber formation did not take place. For this interval, the cylindrical collector was positioned so that bowl was approximately centered on the lower half of the collector. Further detailed observations of the initiation process were discussed previously.[38]

Approximately 10 s after the appearance of full circumferential jets, the voltage level was manually reduced (<5 s) to a constant, lower level (the "working" voltage). Simultaneously, the cylindrical collector was vertically lowered so that the bowl was now centered on the upper half of the collector. During the transition from initiation to operating mode, a fraction of the streaming jets transform into stable, fiber forming spinning jets. The lower electric field amplitude at the working voltage value is insufficient to generate new jets, but as discussed later, jets can be maintained at this level and the field provides for a flow rate (due to the electrostatic suction at the jet) appropriate for fiber formation. The stable spinning jets are directed at ∼30° above horizontal and formed nanofibers that collected on the upper half of the collector. The synchronous repositioning of the collector with the voltage transition ensures that wet solution on the collector (accumulated during the initiation stage) flowing under gravity could not dissolve the high-quality nanofibers (manufactured at a later time under the operating voltage). As reported previously,[38] optimized parameters for the production of nanofibers using bowl electrospinning of 6 wt % PEO solution (solution no. 3) were loading volume of 78 mL and an initiation voltage of 55 kV applied for short time interval ($\Delta t_i \sim 20$ s), before a manual reduction (∼3 s) to a stable operating voltage of 16 kV. Unless otherwise explicitly noted, these parameters were maintained for all bowl electrospinning experiments.

The bowl electrospinning process was imaged using a camcorder (Sony, Model DCR-SR68) with an enhanced viewing lens (Zeiss, 6 mm × 18 mm T monocular) and two digital single lens reflex (SLR) cameras (Olympus, Model E-620, and Canon, Model Rebel T3i). Polymer jets were continuously illuminated by a halogen lamp (Northern Industrial Lighting, Model 1002) and/or a light source comprised of a square array of white LEDs (Visual Instrumentation Corp., Model 900445), where the light orientation was selected, and shadowing baffles were strategically positioned, to reduced glare. The number of stable spinning jets as a function of time was determined by analysis of the time-stamped recorded video.

2.4. Fiber Characterization. A scanning electron microscope (SEM) (JEOL JSM-6400 FE) operating at 5.0 kV was used to study the morphology of nanofibers obtained from TNE and bowl electrospinning experiments. The samples were sputter-coated (Technics Inc., Hummer II) with Au−Pd at a thickness of ∼100 Å in order to create a conductive surface and reduce any charging effects.

Table 2. Nanofiber Production Rate for Bowl Electrospinning Using Different PEO Solutions under an Operating Voltage of 16 kV and a Working Distance of 15 cm, Unless Otherwise Specifically Noted[a]

solution no.	PEO concn (wt %)	concn (wt %) or (v/v)	mass throughput (g/h)	av jets (no.)	mass throughput per jet (g/h)
1+	4		1.01 ± 0.06	21 ± 7	0.048 ± 0.016
1*	4		0.81 ± 0.07	17 ± 4	0.048 ± 0.012
2	5		0.80 ± 0.11	24 ± 5	0.033 ± 0.008
3	6		0.77 ± 0.07	22 ± 5	0.035 ± 0.009
4	7		0.39 ± 0.03	11 ± 10	0.036 ± 0.032
5	6	0.001 NaCl	0.77 ± 0.04	28 ± 7	0.028 ± 0.007
6	6	0.005 NaCl	0.68 ± 0.03	26 ± 4	0.026 ± 0.004
7	6	0.01 NaCl	0.66 ± 0.03	21 ± 8	0.031 ± 0.012
8	6	0.05 NaCl	0.26 ± 0.04	10 ± 7	0.026 ± 0.019
9+	4	0.1 Triton	1.16 ± 0.11	25 ± 12	0.046 ± 0.023
9*	4	0.1 Triton	0.951 ± 0.09	20 ± 9	0.048 ± 0.022
10+	6	0.1 Triton	1.05 ± 0.14	22 ± 7	0.048 ± 0.017
10*	6	0.1 Triton	0.63 ± 0.03	17 ± 5	0.037 ± 0.011
11+	7	0.1 Triton	1.00 ± 0.04	14 ± 7	0.071 ± 0.036
11**	7	0.1 Triton	0.70 ± 0.05	14 ± 6	0.050 ± 0.022
12	7	0.001 NaCl	0.31 ± 0.05	10 ± 8	0.031 ± 0.025

[a]For conditions under which streaming occurred (+ = streaming), the working voltage was reduced to allow quality fiber formation as indicated (* = 15 kV, ** = 14 kV). The average jet number and mass throughput values are calculated from 20 min of continuous spinning.

Revolution software was used to measure the fiber physical characteristics; typically, 25 individual measurements for each sample were used to calculate the mean diameter and estimate the standard deviation. Porosity of the nanofibrous samples was determined by an established protocol:[38,39,52−59] using ImageJ Analyzer software, the SEM images were converted to grayscale and analyzed to identify the top layer of the mat and measure the number of filled (belonging to this first fiber layer) versus unfilled pixels.

After electrospinning for known time intervals, the nanofibrous material production rates were experimentally measured by comparing the weight of the aluminum foil used to collect the mats before and after nanofiber deposition (with a waiting period of 3 h in ambient conditions to ensure the mats were completely dry). Flow rates per jet for bowl electrospinning (comparable to the feed rate in a TNE experiment) were determined from the measured fabrication rate per hour, adjusted by the average measured number of jets over the collection period, and converted to an equivalent solution volume per time (Table 2). Large errors in the number of average jets (or, equivalently, in the mass throughput per jet) indicate reduced jet stability over the 20 min collection period; approaches for optimization of jet stability in edge electrospinning will be addressed in a future work.

2.5. Electric Field Simulations. Using commercially available software (Maxwell 3D, ANSOFT Corp.), the electric field distribution generated within the bowl electrospinning geometry was modeled. Finite element methods and adaptive meshing are utilized by the software to provide a converged solution. The experimental apparatus was simulated by defining a scaled structure using the electrospinning parameters (i.e., applied voltages, working distance, source/collector dimensions, material composition, and polymer fluid within the reservoir). Typical optimized simulation parameters resulted in a minimum (maximum) mesh element dimension of <0.05 mm (0.13 mm) with a total ~10^6 mesh volume elements, where ~30% of these defined the source electrode in order to provide the highest spatial resolution in experimentally important regions. For an operating voltage of 16 kV, the electric field at the bowl-edge is ~3×10^6 V/m (pointing ~40° above the plane of the bowl lip), with a change in the electric field over the first 1 mm of ~2×10^9 V/m^2.

3. RESULTS AND DISCUSSION

3.1. Direct Comparison with TNE: Fiber Quality and Flow Rate. Previous reports[38,39] have demonstrated that spinning from an unconfined fluid near the sharp edge of a flat plate or the bowl lip provides the benefits of multiple jet sites that can spontaneously rearrange as well as the high fiber quality associated with confined feed techniques (i.e., using some form of a nozzle). We refer to these new methods as *edge electrospinning* as the stable spinning sites are located on the fluid surface near a sharp conducting edge. This edge shape creates a strong electric field that lessens dramatically along the path between the source electrode and grounded collector, in a similar manner as the field near the needle tip in TNE falls in the direction of its collector. The edge electrospinning approach in general results in fibers of essentially identical quality as obtained in TNE because of this similarity in the electric field magnitude and gradient; equally important in bowl electrospinning is that the voltage can be facilely tuned so that the electric-field-induced feed rate is also similar to that in TNE. Thus, the polymer solution experiences similar conditions in the edge and TNE schemes, resulting in similar quality fibers. Figure 2 shows representative SEM images of PEO mats comprised of high-quality nanofibers produced from different polymer solutions using the bowl-edge electrospinning method.

Table 3 summarizes fiber diameters and porosity values measured from nanofibrous mats fabricated in either TNE or bowl configurations using the 12 different solutions summarized in Table 1. In nearly all cases, the fiber diameter and spread in fiber diameter distribution from bowl electrospinning are

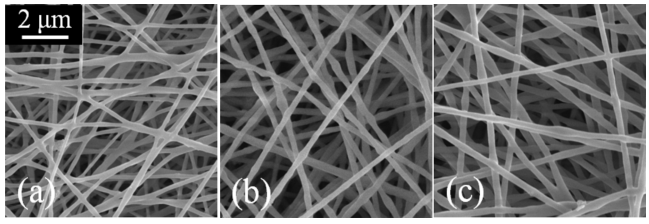

Figure 2. Representative SEM images of nanofibrous mats fabricated from different polymer solutions under similar process parameters demonstrate that the bowl electrospinning technique produces high quality nanofibers ~200 nm in diameter: (a) 5 wt % PEO (solution no. 2), (b) 6 wt % PEO (solution no. 3), and (c) 7 wt % PEO (solution no. 4).

Table 3. Comparison of Fiber Diameters and Porosity Values Determined by SEM Image Analysis of the Nanofibrous Mats Produced by TNE and Bowl Electrospinning for Differing PEO Solutions[a]

			TNE		bowl electrospinning		
solution no.	PEO concn (wt %)	concn (wt %) or (v/v)	fiber diam (nm)	porosity (%)	fiber diam (nm)	porosity (%)	flow rate (μL/min)
1*	4		beads	beads	beads	beads	20.5 ± 5.1
2	5		194 ± 25	80.0 ± 1.0	175 ± 24	79.0 ± 1.0	11.6 ± 2.9
3	6		246 ± 21	75.2 ± 0.5	217 ± 27	73.9 ± 1.5	10.2 ± 2.5
4	7		305 ± 40	76.3 ± 1.0	241 ± 20	76.4 ± 1.7	8.9 ± 8.1
5	6	0.001 NaCl	249 ± 27	75.6 ± 0.5	212 ± 25	75.6 ± 0.4	8.0 ± 2.0
6	6	0.005 NaCl	240 ± 24	76.3 ± 1.2	200 ± 28	78.2 ± 1.3	7.6 ± 1.2
7	6	0.01 NaCl	216 ± 18	77.3 ± 1.0	193 ± 20	75.7 ± 0.5	9.2 ± 3.5
8	6	0.05 NaCl	212 ± 14	77.0 ± 1.1	185 ± 25	76.1 ± 0.8	7.6 ± 5.4
9*	4	0.1 Triton	beads	beads	beads	beads	20.7 ± 9.5
10*	6	0.1 Triton	201 ± 20	76.6 ± 2.9	194 ± 31	72.3 ± 3.7	10.8 ± 3.2
11**	7	0.1 Triton	254 ± 32	75.2 ± 2.2	280 ± 39	73.3 ± 2.3	12.6 ± 5.5
12	7	0.001 NaCl	278 ± 24	75.6 ± 0.8	240 ± 27	76.6 ± 0.5	7.8 ± 6.4

[a]An applied voltage of 11 kV, a working distance of 15 cm, and a feed rate of 5 μL/min were utilized as optimal parameters for TNE; for bowl electrospinning, a working distance of 15 cm and an applied voltage of 16 kV (* = 15 kV, ** = 14 kV) were used. Calculated flow rates are an average per jet (see Table 2 and the associated discussion).

equivalent to or less than that from TNE, demonstrating that the two techniques produce the same high-quality fibers. When the entanglement density is insufficient to form bead-free fibers (e.g., solution no. 1 (9), 4 wt % PEO (4 wt % PEO with surfactant)), this occurs under both electrospinning methods. Similarly, the measured porosity values from the two approaches also match well. Figure 3 graphically displays the trends of the fiber diameter data (fourth column, Table 3) for all the solutions which produced high-quality nanofibers.

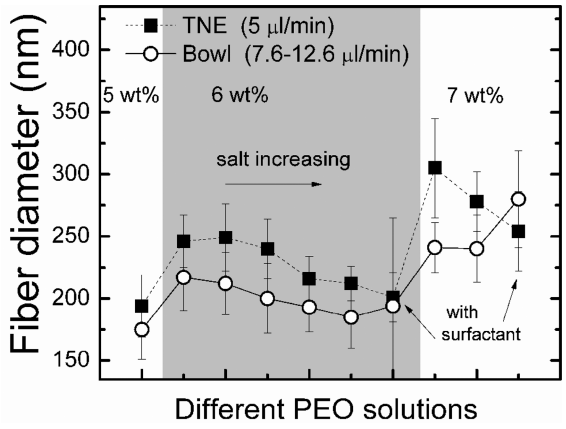

Figure 3. Measured nanofiber diameter for PEO solutions with different properties electrospun using either TNE or bowl approaches. Data taken from Table 3.

Experimentally determined estimates of flow rates per jet under bowl electrospinning (the equivalent of a feed rate in TNE) are summarized in the final column of Table 3. For all experiments using TNE, the externally controlled feed is a fixed rate of 5 μL/min. The flow rate for bowl electrospinning is controlled by the applied electric field at the "working" value, depending on both the velocity induced by the electrostatic shear in the jet and the cross-sectional area of the jet. As discussed in further detail later, the flow rate thus depends on both the viscosity of the solution (which will affect the velocity and jet cross-sectional area for a given electric field) and the critical electric field to form or maintain a jet, which depends on the surface tension of the fluid. Note that the measured flow rates for bowl electrospinning are very similar (although 1.5×–2.5× larger) to the quasi-optimal value for TNE, ranging from about 7.6 to 12.6 μL/min. Thus, it is not only the similarity between the electric field pattern in bowl and TNE configurations, as previously discussed[38] but also the similar feed rate in the two schemes that results in fabrication of similar quality fibers. Thus, two aspects of the bowl edge configuration make it particularly important as a scale-up scheme: the geometrical similarity in the field pattern and the ability (by utilizing two-stage voltage intervals) to tune the "working" flow rate to match an optimal rate for high-quality fiber production.

In Table 3, the working voltage level for solutions no. 10 (6 wt % PEO with surfactant) and no. 11 (7 wt % PEO with surfactant) was 15 and 14 kV, respectively, because streaming of wet fluid to the collector occurred when spinning at the normal working voltage (i.e., 16 kV) due to the low surface tension of these solutions. Even at this reduced operating voltage level, the flow rate for solution no. 11 is elevated (~13 μL/min), and the observed fiber diameter from bowl electrospinning is slightly larger than from optimal TNE (e.g., 5 μL/min), as might be expected for a higher flow rate.

3.2. Number of Fluid Instabilities as a Function of Solution Properties. *3.2.1. A Simple Model for Spontaneous Fingering.* Figure 4 depicts the distinct pattern of jets surrounding the source bowl in bowl-edge electrospinning at the working voltage from a top looking downward perspective

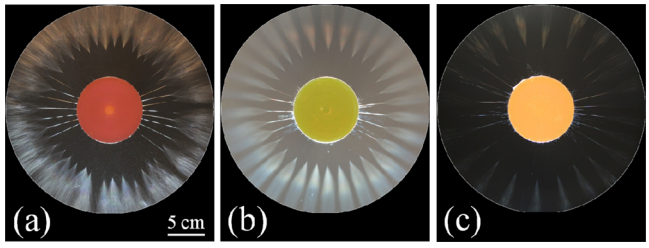

Figure 4. Digital SLR camera image of bowl electrospinning, viewed from the top looking downward after 1 min at the operating voltage of (a) solution no. 9 (4 wt % PEO with surfactant) with 40 jets, (b) solution no. 3 (6 wt % PEO) with 31 jets, and (c) solution no. 4 (7 wt % PEO) with 24 jets. Linear regions, and part of the whipping regions, are clearly visible.

dx.doi.org/10.1021/ma301207t | Macromolecules 2012, 45, 6527–6537

for three different polymer solutions. These images are taken 1 min after reduction to the operating voltage level. In each optical image the interior and edge of the bowl, the protruding fluid jets, the linear region where the fluid/forming fiber is propelled in a direct line, and a portion of the whipping region, are all readily shown; the grounded cylindrical collector, masked to minimize glare from light reflections, is located outside the field of view. The jets form and subsequently reside at the bowl edge, where the electric field is maximized. The jets spontaneously arrange due to electrostatic jet-to-jet repulsion to be roughly equally spaced along the perimeter of the bowl: there are 40 jets for the 4 wt % PEO with surfactant solution (Figure 4a; solution no. 9), 31 jets for the 6 wt % PEO solution (Figure 4b; solution no. 3), and 24 jets for the 7 wt % PEO solution (Figure 4c; solution no. 4).

As shown in Figure 4, the polymer solution properties fundamentally affect the maximum density of jets (or equivalently the characteristic wavelength of the fluid instabilities). We introduce a simple intuitive model (after published work[40,60]) and then progress to compare maximum jet number and time of jet formation in a more complete treatment.[42] Throughout this section, a few well-known properties of Taylor cone systems[47] are utilized. First, for relatively conducting solutions such as those in this work, the fluid is charged, with the charge residing largely on the surface and screening the electric field due to the applied voltage, except in the jet region where the electric field penetrates the solution and electrostatic forces forms the jet; this is the so-called *leaky dielectric* model. Second, we also will use a cone-jet picture where most of the fluid perturbation is static, and significant solution flow only occurs near the apex of the cone (i.e., in the jet region).

A general discussion of fluid fingering due to an applied force has been previously published:[40] in this specific case, the electric field serves to establish the driving force to create fluid perturbations. The outwardly directed force due to the electric field is balanced by the surface tension, which resists deformation of the fluid (and thus an increase in surface area). The balance between these two forces sets a characteristic length scale for the spacing between the fluid fluctuations which will ultimately form jets.

In a simple model, the radial position r of the edge of the fluid around the rim of the bowl varies as

$$r = r_0 + \Delta r \cos\left(\frac{2\pi r_{bowl}\varphi}{\lambda}\right) \tag{1}$$

where r_0 is the equilibrium position of the fluid with respect to the bowl center, Δr is the amplitude of a fluctuation (estimated by imaging individual jets), r_{bowl} is the bowl radius, φ is the angular variable around bowl edge, and λ is the characteristic distance between oscillations. In order to form such perturbations, the fluid flows along the φ direction: that is, fluid is transferred from regions that will ultimately become troughs to regions that become crests. Note: this flow rate per unit film height Q_φ (where height in this case refers to the thickness of the film above the rim of the bowl) is different than the flow rate through a jet in the radial direction Q, which will be discussed later. The rate at which perturbations form is related to the flow rate Q_φ by volume conservation so that as the perturbations form, $-dr/dt = (1/r_{bowl})(dQ_\varphi/d\varphi)$. This flow rate is directly proportional to the net driving force per volume f and the cube of the average film thickness $\tilde{r}$ (where $\tilde{r} = r_0 - r_{bowl}$) and inversely proportional to the viscosity η such that[40] $Q_\varphi \approx \tilde{r}^3 f/3\eta$. On the side of any fluid protrusion, the surface tension force per volume, approximately given as (γ/r_{bowl}^3)-$(\partial^3 r/\partial\varphi^3)$ where γ is the surface tension, will be directed away from the protrusion (toward a trough), tending to restore the film to smooth surface (i.e., relax the protrusions). The force due to the electric field can be calculated from the change in electrostatic pressure with φ (as $^1/_2\varepsilon_0 E^2$ where ε_0 is the permittivity of free space and E is the electric field at the edge of the fluid), resulting in the expression $(\varepsilon_0 E/r_{bowl})(\partial E/\partial\varphi)$. In the bowl geometry, E depends on the distance from the bowl edge, so that $E \approx E_0 + (\partial E/\partial r)\Delta r \cos(2\pi r_{bowl}\varphi/\lambda)$. Combining these equations yields a time-dependent expression for Δr as the perturbations form, namely

$$\frac{d(\Delta r)}{dt} = \frac{\tilde{r}^3}{3\eta}\Delta r\left(\frac{2\pi}{\lambda}\right)^2\left[\varepsilon_0 E_0\frac{\partial E}{\partial r} - \gamma\left(\frac{2\pi}{\lambda}\right)^2\right] \tag{2}$$

which has an exponential solution with a characteristic time constant τ:

$$\tau = \frac{3\eta}{\tilde{r}^3}\left(\frac{\lambda}{2\pi}\right)^2\left[\varepsilon_0 E_0\frac{\partial E}{\partial r} - \gamma\left(\frac{2\pi}{\lambda}\right)^2\right]^{-1} = \frac{3\eta}{\gamma\tilde{r}^3}\frac{1}{q^2(\kappa^2 - q^2)} \tag{3}$$

where the wavenumber $q = 2\pi/\lambda$ and $\kappa = [(\varepsilon_0 E_0/\gamma)(\partial E/\partial r)]^{1/2}$.

Equation 3 shows that each characteristic wavelength has a distinct τ value. If τ is positive ($q^2 < \kappa^2$), perturbations having such a wavelength will grow exponentially in time. This occurs for sufficiently long wavelengths (low q values). As the electric field magnitude E and/or electric field gradient $\partial E/\partial r$ increases, shorter wavelengths are allowed, resulting in more jet sites in this case. In contrast, λ values associated with negative τ (short wavelength oscillations, when $q^2 > \kappa^2$) are exponentially damped. Equation 3 can be used to determine the fastest growing wavelength (that is, the one having the minimum τ value or shortest time for formation) as

$$\lambda = 2\pi\sqrt{\frac{2\gamma}{\varepsilon_0 E_0\left(\frac{\partial E}{\partial r}\right)}} = 2\pi\frac{\sqrt{2}}{\kappa} \tag{4}$$

A similar treatment has previously been utilized to estimate the wavelength of perturbations within other fiber forming techniques.[40,60]

Equation 4 provides a framework to understand the basic parameters which determine the maximum jet number under bowl electrospinning. As the electric field near the edge of the bowl E_0 and/or the gradient $\partial E/\partial r$ in moving from the bowl edge to the collector increase, the solution is forced to tolerate a greater number of jets or equivalently, a closer jet spacing (i.e., having a smaller λ). In contrast, a higher surface tension will decrease the number of jets (i.e., requiring a larger λ). Although the solution viscosity and effective thickness of the fluid film protruding from the bowl ($\tilde{r}$) affect the dynamics of instability formation (i.e., see eq 3), they do not directly affect the jet number in this simple model. Utilizing the measured value of the solution's surface tension as well as E and $\partial E/\partial r$ from the electric field simulation eq 4 yields $\lambda = 9.4$ mm for a 6 wt % PEO solution (solution no. 3). This result is consistent with the measured λ value of 8.8 ± 0.8 mm from the maximum number of jets (~32 ± 3, averaged over three experiments, e.g., as shown in Figure 4b) and the known physical radius of the bowl.

dx.doi.org/10.1021/ma301207t | Macromolecules 2012, 45, 6527–6537

3.2.2. Jet-to-Jet Interactions. In addition to these fluid−field interactions, when electrospinning under conditions having densely packed jets, jet-to-jet interactions (i.e., the electrostatic repulsion between neighboring charged jets) become important. In the cylindrically symmetric bowl geometry, jet-to-jet interactions lead to two notable effects: (i) self-adjusting equal jet spacing along the bowl edge and (ii) a compression of the jet profile, which tends to limit the total jet number. We discuss each of these developments. First, consider a single jet having adjacent neighbors located at higher and lower φ (e.g., to the "left" and "right"). The force due to each jet neighbor is directed perpendicularly (along a straight line) from the neighbor. Thus, the neighbor located at lower φ exerts a force on the jet directed toward higher φ, until perfectly balanced by the force toward lower φ exerted by the other neighbor at higher φ: as expected, this equilibrium results in equally spaced jets around the bowl.

There is a second effect of jet-to-jet interaction: because of the repulsive force between jet neighbors, jets reorganize by moving charge closer to the jet axis to minimize electrostatic interaction (i.e., jets are observed to narrow in cross section). Experimentally, we find that the jet diameter is strongly dependent on viscosity. For high-viscosity fluids, the transition in velocity from a maximum at the jet apex to essentially zero velocity at the edge of the Taylor cone requires a longer distance; thus higher viscosity fluids produce wider jets. Conversely, when a high-viscosity jet is compressed by jet-to-jet interactions, the compressed jet may only be able to support a lower maximum velocity, which may lead to jet instability. This effect can be estimated[40] as the viscous force per volume in the circumferential φ direction (perpendicular to the flow) is given by $\sim(\eta/r_{bowl}^2)(\partial^2 v/\partial\varphi^2)$ and balanced by the compressive jet-to-jet interaction force. Estimating the surface charge on the fluid (see below) and utilizing the measured diameter D and the amplitude Δr of a conical jet to find ρ, the estimated charge on each jet, the standard charge−charge interaction form results in an electrostatic force per unit volume of $(1/4\pi\varepsilon_0)[\rho^2/(\lambda - D)^2](2/V_{jet})$, where V_{jet} is the volume of a conical shaped jet and $(\lambda - D)$ is the distance between the edges of neighboring cones. Surface charge density can be roughly estimated as $\varsigma C/\Sigma$, where ς is the electrostatic potential of the bowl, C is the capacitance of the bowl−collector system as determined by computational modeling, and Σ is the surface area where most of the pertinent surface charge is located (one-half the surface area of a cylindrical fluid strip of height h (the distance of the fluid above the lip of the bowl) at the circumference $2\pi r_{bowl}$). Estimating[40] the second derivative of the velocity in the circumferential direction as $v/(D/2)^2$ yields

$$\frac{4\eta v}{D^2} = \frac{1}{4\pi\varepsilon_0}\frac{2\rho^2}{V_{jet}(\lambda - D)^2} \tag{5}$$

Equation 5 provides a general estimate of the λ values at which jet-to-jet interactions will begin to impede flow due to jet compression, consequently decreasing jet stability. By introducing a minimum stable velocity v (below which the jet would extinguish), eq 5 sets a limit on the maximum number of jets, independent of the limit determined by eq 4, and reflecting only the effect of jet-to-jet interactions. The largest λ value—determined by force balance with surface tension (eq 4) or, alternatively, by examination of the viscoelastic forces in the circumferential direction (eq 5)—should be experimentally observed. For example, solving eq 5 for λ given a characteristic cone-jet diameter, amplitude (~100 μm), viscosity, and minimum velocity (1 mm/s as determined from jet stability studies), reveals that jet-to-jet interactions are not important for the 6 wt % PEO solution (solution no. 3; jet diameter 430 μm) above a λ value of ~6 mm, which is less than the limit predicted from a surface tension analysis (~9 mm); thus, jet-to-jet interactions play no role in such a case. In contrast, as discussed below, for spinning solutions with low surface tension but high viscosity (such as solution no. 11, comprised of 7 wt % PEO with surfactant), jet-to-jet interactions may significantly limit the maximum jet number experimentally observed.

3.2.3. Experimental and Theoretical Comparison of Jet Number. To make additional direct comparisons with experimentally measured quantities, we now discuss a more complete model to predict λ (when neglecting jet-to-jet interactions) and the rate at which fluid perturbations form. Previously published work treated the case of a thin layer of fluid uniformly coating a sphere which is placed at high voltage relative to ground.[42] For this case, when the fluid layer is much smaller than the sphere radius, the perturbation growth rate σ for each characteristic number of perturbations is given by

$$\sigma = \frac{\gamma}{2\eta r}\Lambda(n)[n + 2 - F]\varepsilon^2 \tag{6}$$

where r is the sphere radius and ε is the relative fluid film thickness normalized by r. Λ, a numerical factor which likely to differ in the present case due to the different geometry, and F (which represents the ratio between electrostatic and surface tension forces) are each given by

$$\Lambda(n) = \frac{n(n^2 - 1)(2n + 1)}{2n^2 + 4n + 3} \qquad F = \frac{\varepsilon_0}{\gamma} r\tilde{E}^2 \tag{7}$$

where the F equation is modified to reflect the electric field in the radial direction $\tilde{E}$, rather than the applied voltage, which enables application of the expression to our alternative geometry. In eq 7, n is the number of perturbations on a half-sphere (hence, the experimental value is twice this). Equation 6 provides the rate at which instabilities with a particular characteristic number of jets (or jet spacing) arise. The n value at which $-\sigma$ peaks provides the expected number of jets for a given situation (or, equivalently, $\lambda = (2\pi r_{bowl}/2n)$; the $-\sigma$ value at the peak is the rate at which instabilities will form (equivalently, the average time after application of the voltage before instabilities develop is $\tau \sim -1/\sigma$).

In the model summarized in eqs 6 and 7, the n value at which the fastest rate occurs (the extremum value) depends on the electric field and surface tension values (in agreement with the simpler model) and the characteristic radius r and is independent of solution viscosity and film thickness as expected. (However, the latter two quantities do strongly influence the rate of instability formation.) Setting $r = r_{bowl}$, and utilizing the measured surface tension value and the value of $\tilde{E}$ (at 16 kV, $\sim 2 \times 10^6$ V/m) from our computational simulations, we calculate the expected jet number for the 6 wt % PEO solution (solution no. 3) at this operating voltage as 34 jets, which matches well with the experimental value of 32 ± 2 jets. Given the difference in the spinning geometries, this agreement is possibly coincidental; however, the spherical model is helpful in understanding the trends in the experimental data. Figure 5 summarizes the comparison between the film-covered sphere model, the simpler model in section 3.2.1, and experimental

dx.doi.org/10.1021/ma301207t | Macromolecules 2012, 45, 6527−6537

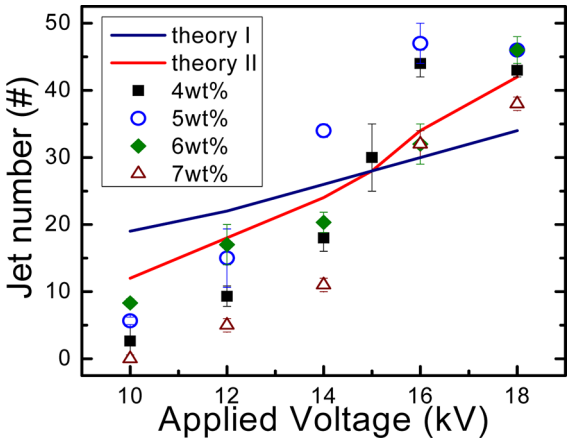

Figure 5. Experimentally observed jet number (1 min into the working regime; an average of >3 experimental runs) as a function of applied voltage for PEO solutions with 4−7 wt % (solutions 1−4). The theory I estimate is derived from eq 4, and the theory II estimate is from eqs 5 and 6. The error on the theoretical estimate is ±2 jets.

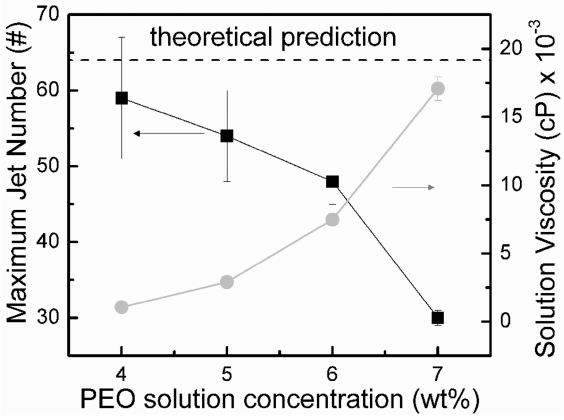

Figure 6. Maximum jet number (black squares, left ordinate) and viscosity (gray circles, right ordinate) as a function of polymer concentration for solutions with added surfactant (0.1 wt % Triton X-100). Note: the measured surface tension of both the 4 and 5 wt % PEO solutions is ∼32 mN/m.

observations of maximum jet number (at 1 min into the working regime) as a function of applied working voltage in bowl electrospinning.

Both models predict values that are the same order of magnitude as the experimental data, but the spherical model yields better agreement. For instance, the predicted value of 24 jets at 14 kV is applicable for PEO solutions at all polymer concentrations and salt contents without surfactant (solutions 1−8, 12), as surface tension is independent of these parameters. Experimental observations of maximum jet number for these cases range from 11 to 34. We note that the highest viscosity solution (i.e., that with the highest polymer concentration of 7 wt % PEO) consistently had fewer jets than lower viscosity solutions, which indicates that flow rate or solution velocity (which is higher for low-viscosity solutions) may enhance jet stability. It is possible that jet-to-jet interactions are also important for these 7 wt % PEO solutions.

We can further compare our experiment with the film-covered sphere model by altering the surface tension and observing the results. When surface tension is reduced with the addition of surfactant, the results from the theoretical models are systematically higher than the experimental results. Figure 6 depicts results obtained for solutions of 4−7 wt % PEO with surfactant (solutions 9−11 in addition to a 5 wt % PEO with surfactant solution used for only this particular comparison). For 6 wt % PEO solution with surfactant (solution no. 10) at 16 kV, the film-covered sphere model predicts 64 jets (λ = 4.4 mm) and 48 ± 3 (λ = 5.9 mm) are observed. The 7 wt % solution with surfactant (solution no. 11) has even poorer performance (Figure 6). Notably, as the concentration (and thus the viscosity) decreases, the number of observed jets rises (even though the surface tension for all solutions is approximately the same). The film-covered sphere model does not account for jet-to-jet interactions, but we can estimate their effect by utilizing eq 5 which gives the λ value below which (for a given cone-jet diameter D and velocity v) the jet-to-jet interaction would limit the total number of jets. Taking the most extreme case, for the 7 wt % solution with surfactant (solution no. 11) at 16 kV, the diameter D = 625 μm. Using a minimum fluid velocity below which jets are unstable (determined from the measured flow rate per jet for cases of unstable spinning solution/voltage regimes) of ∼1 mm/s yields $\lambda_{\text{jet-to-jet}}$ = 8.3 mm (or 34 jets), which better matches the experimental result of 30 ± 1 jets. This outcome indicates that jet-to-jet interactions serve as the overall jet number limiting factor for conditions when (1) the solution viscosity is high, resulting in broad cone-jet profiles, and (2) the solution surface tension is low and thus does not restrict the number of jets. To test this hypothesis, we utilized solutions of 4 or 5 wt % PEO with surfactant. In these cases, the viscosity is sufficiently low so that experimentally observed cone-jet diameters are small (∼100 μm), and thus jet-to-jet interactions should be minimized. As shown in Figure 6, as the solution viscosity is reduced, the jet number reverts to the value predicted by the surface-tension-dominated sphere model, as the effect of jet-to-jet interactions is no longer a limiting factor.

3.3. Characteristic Time of Instability Formation: Utilizing Two-Stage Voltage. The previous calculations utilized the electric field in the working region as a parameter to predict the jet number present at the applied operating voltage. However, these jets are not formed at this working voltage level but rather develop during the initiation voltage interval; thus, the dynamics of jet formation are determined by the initiation voltage. The need for a higher amplitude initiation voltage is clearly seen by examining the σ (rate of instability development) values for these peak n quantities at both operating and initiating voltage. Experimentally, we observe the average time between the application of voltage and the appearance of the first spontaneous jet; these τ values are proportional to viscosity as predicted by both eq 3 and 6 and range from 0.5 to 4 s depending on solution concentration. Utilizing these measured values and eq 6, the best fit occurs for an effective film thickness $\varepsilon r_{\text{bowl}}$ of ∼50 μm, which is reasonable from observation of side-on images of the bowl during jet formation. For simplicity, we utilize this value for all calculations in this section although it is likely to vary somewhat with solution parameters and applied voltage. Thus, for instance, for the 6 wt % PEO solution (solution no. 3) the $-\sigma$ peak value at the initiating voltage (55 kV) is 0.49 s^{-1} or a τ = 2.0 s, which matches the experimental value of 2 ± 1 s. Increasing the viscosity slows the process, with a predicted value of 4.6 s for the 7 wt % PEO solution (solution no. 4), again matching the empirically measured value of 4 ± 3 s. In contrast, the τ values at the operating voltage (16 kV) for these two solutions are predicted to be 4700 and 10 700 s,

dx.doi.org/10.1021/ma301207t | Macromolecules 2012, 45, 6527−6537

respectively, which is on the order of hours. Such long initiation times mean that jet formation is extremely unlikely at the operating voltage and is not experimentally observed, even for the lowest concentration (lowest viscosity) and lowest surface tension solutions. Thus, many jets ($2n \approx 240$ from the sphere-coated model, although this number is likely limited by jet-to-jet interactions) formed at the initiating voltage transform into fewer, stable jets as the voltage is reduced to the working value.

This analysis highlights the implicit advantage of the two-stage voltage system; many jets are formed quickly at the initiation voltage (even for highly viscous solutions), and the jet number reduces when lowering the applied voltage amplitude (to a final value of the working voltage), with these remaining jets quasi-stable for an extended period of time. (For example, even with a single batch operation of the bowl, where fluid loss due the lack of a refill mechanism may eventually lead to jet destabilization, at least 50% of jets are still present after 20 min of continuous spinning.) Notably, if only the working voltage level was applied, jets would never generate (i.e., the time for jet formation would be prohibitively long). Furthermore, by utilizing the working voltage, the desirable feed rate appropriate for high-quality fiber formation can be selected.

3.4. Electrospinning in the Subcritical Regime. The observations in the previous section can be further understood by considering the critical electric field needed to form a single jet. (Published work has presented such estimates for an electric field working directly against gravity to form a fluid instability or jet;[41] however, these results are not applicable to our case due to the absence of a significant contribution from gravity.) One previous report modeled formation of a jet from a single droplet of radius a, supported by a substrate, finding $E_{critical} = 0.86\ (\gamma/a\varepsilon_0)^{1/2}$ and producing numerical estimates for Q, the flow rate (per jet) as a function of applied electric field above and below this value.[61] This form for $E_{critical}$ can be obtained (within a numerical factor ~1) from eq 4 by setting $r_{bowl} = a$ (making a single droplet), the jet number to 1 ($\lambda = 2\pi r_{bowl}$), and approximating $\partial E/\partial r \sim E_0/r_{bowl}$. Hysteresis effects in the formation and maintenance of Taylor cones have long been reported and studied.[46−49] In general, a larger applied voltage or field is required to form a Taylor cone than that needed to sustain it. Thus, after formation at an electric field above $E_{critical}$, the field can be reduced significantly while maintaining the jet. At a voltage level significantly lower than $E_{critical}$ the flow rate through the jet goes to zero and the jet collapses[61] (see section 3.5). Calculating $E_{critical}$ for the 6 wt % PEO solution (solution no. 3), using the characteristic radius of the fluid perturbation (215 μm) as a, yields a critical value of 4.8×10^6 V/m, which is below the electric field during initiation (1.4−2.1 times smaller) and about 1.5−2.5 times larger than the field at the operating voltage. Even at the reduced surface tension when surfactant is present, the critical field (3.5×10^6 V/m) is still larger than that under operating conditions. Thus, as we observe experimentally, the electric field at the working voltage is not sufficient to form jets; rather, it serves only to maintain the jets formed at the initiation voltage. Such hysteretic effects enable quick, efficient formation of jets at the elevated initiation voltage and then significant tuning of the working electric field to an appropriate flow rate, as discussed in the next section.

3.5. Tuning the Flow Rate per Jet with the Electric Field. We now examine the experimentally measured dependence of the flow rate per jet Q on the applied electric field and the solution parameters. In bowl electrospinning, the flow rate is determined solely by the interaction between the field and solution; that is, there is no significant additional driving force, such as gravity. Just as in TNE, the flow rate plays a crucial role in determining fiber quality. If the velocity is too high, the polymer stream will not dry sufficiently before reaching the collector and the whipping instability may be lessened, or in the extreme case, wet solution propels directly to the collector ("streaming"). Such streaming events occur for the higher voltage cases shown in Figure 5 for lower viscosity solutions (such as the 4 wt % PEO solution (solution no. 1) at when operated at 16−18 kV). Thus, fiber formation is not possible under these conditions and lower voltages, with correspondingly lower maximum jet number, are required. As discussed in section 3.1, even slight changes in flow rate can increase fiber diameter even when streaming is absent.

The net fluid velocity through the jet (which changes with distance from the bowl or substrate as the jet thins) multiplied by the appropriate jet cross-sectional area results in the effective feed rate per jet (as Q is constant along the jet). Both the velocity and the cross-sectional area are dependent on the electric field and the solution properties. In an analogous system of electro-osmotic flow along a solid surface (where the fluid velocity is constant with position), the net velocity of the fluid is given by $v = \chi\varepsilon_0 E\varsigma/\eta$, where v is the average fluid velocity, $\chi\varepsilon_0$ is the dielectric constant of the fluid, ε_0 is the dielectric permittivity of free space, ς is the electrostatic potential of the surface, E is the electric field, and η is the viscosity.[40] The most important qualities of this equation are a quadratic dependence on the electric field (as the electrostatic potential also changes in proportion to an electric field) and an inverse dependence on viscosity. In another example, the velocity of fluid (at the base of the cone) pulled by an electric field above the critical value (see section 3.4) from a single supported drop[61] is $v \approx \varepsilon_0 E^2 a/\eta$, where a is the radius of the original droplet before the cone-jet was formed. The shape of the jet also changes with applied voltage and with solution parameters. The dependence of jet cross-sectional area on solution and electric field parameters is complex: the clearest trend in the experimental jet diameter is an increase with increasing polymer solution viscosity.

Figure 7 depicts the experimentally determined flow rates for the 4, 5, and 6 wt % PEO solutions (solutions 1−3). As seen in the data, the characteristic jet size is crucial in determining the flow rate: for instance, even though the viscosity increases by ~2.6× between the 5 wt % (open blue circles) and 6 wt % (filled green diamonds) solutions, which should result in a decrease in fluid velocity by this same factor, the increase in experimentally measured jet diameter (from ~260 to 430 μm) results in similar flow rates for the two cases. (In keeping with the model where flow only occurs in the central region of the cone jet, we utilize the jet diameter (the diameter of the cone jet 100 μm from the bowl edge) in this discussion, which is a measure of the cross-sectional area through which flow is occurring, rather than D, the full diameter of the cone jet.) As another example (not shown in Figure 7) the flow rate for the 7 wt % PEO solution (solution no. 4) is ~2.5 μL/min at 12 kV (the lowest experimental value as the jet number at 10 kV is zero) and saturates at ~9.0 μL/min at 14 kV and above—again exhibiting more complex behavior than expected from the simple E^2/η dependence. The fit lines in Figure 7 utilize the form $Q \approx \varepsilon_0 E^2 \pi a^3/\eta$, with a values that increase with viscosity as discussed in the caption. We have chosen this equation for simplicity and set the cross-sectional area radius equal to that of

dx.doi.org/10.1021/ma301207t | Macromolecules 2012, 45, 6527−6537

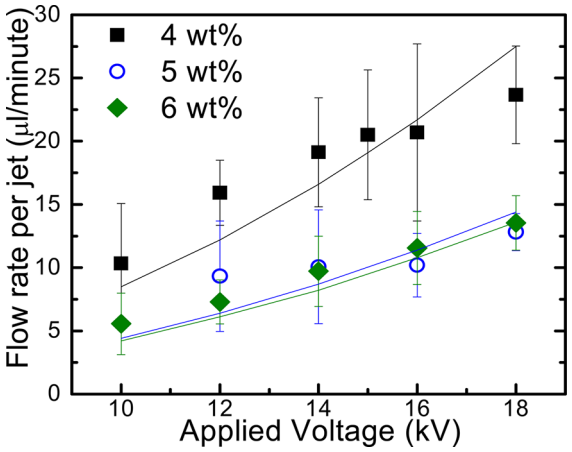

Figure 7. Experimentally determined flow rate as a function of solution type and applied voltage. The solid lines are fits with a = 230, 260, and 350 μm for the 4, 5, and 6 wt % solutions. a was held constant with voltage, and the cross-sectional area was assumed to be πa^2 to minimize the number of free variables (to one) given the sparseness of the data. The a values are larger than the experimentally observed jet radius but follow the same qualitative trend.

the original droplet to limit the number of free parameters to one.

As a complementary approach, the numerical data summarized in previously published work[61] can be compared with the experimental results in order to better explore the subcritical regime where a steeper than quadratic dependence of Q on E is expected, as the jet eventually collapses at sufficiently low voltage. In this work, E is scaled by the electric field value $(\gamma/\varepsilon_0 a)^{1/2}$. The flow rate Q is scaled by a characteristic flow rate which depends on the characteristic velocity in the system (γ/μ) and the cross-sectional area of the droplet (πa^2). Q is essentially independent of solution conductivity for our range of conductivity values. For the 6 wt % PEO solution (solution no. 3), these forms yield a dimensionless electric field of $E \sim 0.5$ (a = 215 μm, which is the radius of the experimentally observed cone jet for this case) for an applied voltage of 16 kV. Reading from the published figure,[61] we find a scaled Q value of ~0.2−0.3, which gives Q = 14−21 μL/min for the 6 wt % PEO solution (solution no. 3), which is similar to the experimental value of 10.2 ± 2.5 μL/min.

The importance of the jet diameter when altering solution properties can be seen clearly from this model. When the surface tension is reduced, one might naively expect a concurrent reduction in the critical electric field (which depends on the square root of surface tension) and thus an increase the scaled E value and Q. However, the jet diameter may also decrease with surface tension, effectively canceling at least a portion of the change. For instance, experimentally, the flow rate per jet for 5 wt % PEO solution (solution no. 2) at 16 kV is 11.6 ± 2.9 μL/min, which overlaps that for the same solution with surfactant (from Figure 7) 12 ± 5 μL/min; even though the surface tension was reduced by 2× (to ~30 mN/m), the jet diameter also decreased by ~2× (from 260 to 130 μm).

Low flow rates occur when a significant amount of salt is added to the polymer solution (e.g., for 6 wt % PEO, solutions 5−8), generally falling below ~8 μL/min at 16 kV. As is well-known, jet diameter narrows with NaCl doping;[62−64] however, even accounting for diameter decrease, fluid velocities also decrease, indicating that the application of the electrostatic force to pull fluid from the jet may be affected in high salt cases.

4. CONCLUSION

Bowl-based edge electrospinning provides a useful scale-up approach of single-needle electrospinning to produce high-quality nanofibers, simply and with demonstrated scaling of 40× in a single batch (i.e., a one-time filling of the bowl) system with a small bowl. We have presented models for use in the prediction of jet number: generally, the lowest viscosity (to minimize jet-to-jet interactions) and lowest surface tension (to maximize the number of jets) provides the highest throughput. On the other hand, in order to maintain high quality (i.e., dry and nonbeaded) nanofibers both viscosity (polymer concentration to ensure sufficient entanglement) and surface tension (to avoid beading) cannot be reduced below certain minimum values. These upper and lower limits set the range for edge electrospinning in a similar manner as in TNE. The importance of jet-to-jet interactions, which are generally mentioned in experimental and theoretical treatments but not quantified, is emphasized in this work, and understanding of this effect is crucial to obtain full experimental and commercial realization. Simple reduction in surface tension is not sufficient to guarantee higher jet number, rather the viscosity of the solution must also be considered, within the limits of the desired fiber quality. Similarly, the importance of cone-jet diameter, which alters flow rate from the simplest prediction and plays a crucial role in jet-to-jet interactions, must also be addressed. Because of the unique two-stage voltage approach employed here, many jets can quickly be formed, stabilize, and organize. Then the voltage can be reduced to a much lower working value where flow rate is appropriate for high-quality fiber formation and hysteretic effects maintain the existing cone jets. In summary, beyond its technological importance, bowl-edge electrospinning provides a scheme to test fluid−electric field interactions and refine and develop models to predict the number of fluid instabilities and the flow through each cone jet.

■ AUTHOR INFORMATION

Corresponding Author

*E-mail: liclarke@ncsu.edu.

Notes

The authors declare no competing financial interest.

■ ACKNOWLEDGMENTS

This work was supported by NSF CMMI-0800237 and the Faculty Research and Professional Development Fund at NC State University. The authors thank Karen Daniels for discussions on fluid fingering; Judy Elson and Chuck Mooney for assistance on the SEM measurements; Wendy Krause, Julie Willoughby, and Xiangwu Zhang for use of instrumentation to characterize polymer solution properties; and NCSU libraries and Amsarani Ramamoorthy for use of digital SLR cameras.

■ REFERENCES

(1) Burger, C.; Hsiao, B. S.; Chu, B. *Annu. Rev. Mater. Res.* **2006**, *36*, 333−368.

(2) Kim, J. S.; Reneker, D. H. *Polym. Compos.* **1999**, *20* (1), 124−131.

(3) Ramakrishna, S.; Fujihara, K.; Teo, W. E.; Yong, T.; Ma, Z. W.; Ramaseshan, R. *Mater. Today* **2006**, *9* (3), 40−50.

(4) Sill, T. J.; von Recum, H. A. *Biomaterials* **2008**, *29* (13), 1989−2006.
(5) Thavasi, V.; Singh, G.; Ramakrishna, S. *Energy Environ. Sci.* **2008**, *1* (2), 205−221.
(6) Jayaraman, K.; Kotaki, M.; Zhang, Y. Z.; Mo, X. M.; Ramakrishna, S. *J. Nanosci. Nanotechnol.* **2004**, *4* (1−2), 52−65.
(7) Kumbar, S. G.; James, R.; Nukavarapu, S. P.; Laurencin, C. T. *Biomed. Mater.* **2008**, *3* (3), 15.
(8) Liang, D.; Hsiao, B. S.; Chu, B. *Adv. Drug Delivery Rev.* **2007**, *59* (14), 1392−1412.
(9) Nair, L. S.; Bhattacharyya, S.; Laurencin, C. T. *Expert Opin. Biol. Ther.* **2004**, *4* (5), 659−668.
(10) McCullen, S. D.; Ramaswamy, S.; Clarke, L. I.; Gorga, R. E. *Wiley Interdiscip. Rev.: Nanomed. Nanobiotechnol.* **2009**, *1*, 369.
(11) Agarwal, S.; Wendorff, J. H.; Greiner, A. *Polymer* **2008**, *49* (26), 5603−5621.
(12) Barnes, C. P.; Sell, S. A.; Boland, E. D.; Simpson, D. G.; Bowlin, G. L. *Adv. Drug Delivery Rev.* **2007**, *59* (14), 1413−1433.
(13) Goldberg, M.; Langer, R.; Jia, X. Q. *J. Biomater. Sci., Polym. Ed.* **2007**, *18* (3), 241−268.
(14) Liao, S.; Li, B. J.; Ma, Z. W.; Wei, H.; Chan, C.; Ramakrishna, S. *Biomed. Mater.* **2006**, *1* (3), R45−R53.
(15) Murugan, R.; Ramakrishna, S. *Tissue Eng.* **2006**, *12* (3), 435−447.
(16) Murugan, R.; Ramakrishna, S. *Tissue Eng.* **2007**, *13* (8), 1845−1866.
(17) Pham, Q. P.; Sharma, U.; Mikos, A. G. *Tissue Eng.* **2006**, *12* (5), 1197−1211.
(18) Schiffman, J. D.; Schauer, C. L. *Polym. Rev.* **2008**, *48* (2), 317−352.
(19) Thomas, V.; Dean, D. R.; Vohra, Y. K. *Curr. Nanosci.* **2006**, *2* (3), 155−177.
(20) Vasita, R.; Katti, D. S. *Int. J. Nanomed.* **2006**, *1* (1), 15−30.
(21) Venugopal, J.; Low, S.; Choon, A. T.; Ramakrishna, S. *J. Biomed. Mater. Res., Part B* **2008**, *84B* (1), 34−48.
(22) Weigel, T.; Schinkel, G.; Lendlein, A. *Expert Rev. Med. Devices* **2006**, *3* (6), 835−851.
(23) Xie, J. W.; Li, X. R.; Xia, Y. N. *Macromol. Rapid Commun.* **2008**, *29* (22), 1775−1792.
(24) Yoo, H. S.; Kim, T. G.; Park, T. G. *Adv. Drug Delivery Rev.* **2009**, *61* (12), 1033−1042.
(25) Frenot, A.; Chronakis, I. S. *Curr. Opin. Colloid Interface Sci.* **2003**, *8* (1), 64−75.
(26) Greiner, A.; Wendorff, J. H. *Angew. Chem., Int. Ed.* **2007**, *46* (30), 5670−5703.
(27) Huang, Z. M.; Zhang, Y. Z.; Kotaki, M.; Ramakrishna, S. *Compos. Sci. Technol.* **2003**, *63* (15), 2223−2253.
(28) Li, D.; Xia, Y. N. *Adv. Mater.* **2004**, *16* (14), 1151−1170.
(29) Reneker, D. H.; Yarin, A. L.; Zussman, E.; Xu, H. Electrospinning of nanofibers from polymer solutions and melts. In *Advances in Applied Mechanics*; Aref, H., VanDerGiessen, E., Eds.; Elsevier Academic Press: San Diego, 2007; Vol. *41*, pp 43−195.
(30) Teo, W. E.; Ramakrishna, S. *Nanotechnology* **2006**, *17* (14), R89−R106.
(31) Reneker, D. H.; Yarin, A. L. *Polymer* **2008**, *49* (10), 2387−2425.
(32) Luo, C. J.; Stoyanov, S. D.; Stride, E.; Pelan, E.; Edirisinghe, M. *Chem. Soc. Rev.* **2012**, *41* (13), 4708−4735.
(33) Yu, D. G.; Branford-White, C. J.; Chatterton, N. P.; White, K.; Zhu, L. M.; Shen, X. X.; Nie, W. *Macromolecules* **2010**, *43* (24), 10743−10746.
(34) Yu, D. G.; Lu, P.; Branford-White, C.; Yang, J. H.; Wang, X. *Nanotechnology* **2011**, *22* (43), 7.
(35) Yu, D. G.; White, K.; Yang, J. H.; Wang, X.; Qian, W.; Li, Y. *Mater. Lett.* **2012**, *67* (1), 78−80.
(36) Dosunmu, O. O.; Chase, G. G.; Kataphinan, W.; Reneker, D. H. *Nanotechnology* **2006**, *17* (4), 1123−1127.
(37) Varabhas, J. S.; Chase, G. G.; Reneker, D. H. *Polymer* **2008**, *49* (19), 4226−4229.
(38) Thoppey, N. M.; Bochinski, J. R.; Clarke, L. I.; Gorga, R. E. *Nanotechnology* **2011**, *22* (34), 11.
(39) Thoppey, N. M.; Bochinski, J. R.; Clarke, L. I.; Gorga, R. E. *Polymer* **2010**, *51*, 4928.
(40) de Gennes, P.-G.; Brochard-Wyart, F.; Quere, D. *Capillarity and Wetting Phenomena*; Springer: New York, 2010.
(41) Lukas, D.; Sarkar, A.; Pokorny, P. *J. Appl. Phys.* **2008**, *103* (8), 7.
(42) Miloh, T.; Spivak, B.; Yarin, A. L. *J. Appl. Phys.* **2009**, *106* (11), 8.
(43) Elmarco http://www.elmarco.com/.
(44) Zhou, F. L.; Gong, R. H.; Porat, I. *Polym. Int.* **2009**, *58* (4), 331−342.
(45) Niu, H. T.; Lin, T. *J. Nanomater.* **2012**, 13.
(46) Cloupeau, M.; Prunetfoch, B. *J. Electrost.* **1989**, *22* (2), 135−159.
(47) de la Mora, J. F. *Annu. Rev. Fluid Mech.* **2007**, *39*, 217−243.
(48) Higuera, F. J. *J. Fluid Mech.* **2010**, *648*, 35−52.
(49) Smith, D. P. H. *IEEE Trans. Ind. Appl.* **1986**, *22* (3), 527−535.
(50) Yu, D. G.; Chatterton, N. P.; Yang, J. H.; Wang, X.; Liao, Y. Z. *Macromol. Mater. Eng.* **2012**, *297* (5), 395−401.
(51) Yu, D. G.; Williams, G. R.; Gao, L. D.; Bligh, S. W. A.; Yang, J. H.; Wang, X. *Colloids Surf., A* **2012**, *396*, 161−168.
(52) Maity, S.; Downen, L. N.; Bochinski, J. R.; Clarke, L. I. *Polymer* **2011**, *52* (7), 1674−1685.
(53) McCullen, S. D.; Stano, K. L.; Stevens, D. R.; Roberts, W. A.; Monteiro-Riviere, N. A.; Clarke, L. I.; Gorga, R. E. *J. Appl. Polym. Sci.* **2007**, *105* (3), 1668−1678.
(54) McCullen, S. D.; Stevens, D. R.; Roberts, W. A.; Clarke, L. I.; Bernacki, S. H.; Gorga, R. E.; Loboa, E. G. *Int. J. Nanomed.* **2007**, *2* (2), 253−263.
(55) McCullen, S. D.; Stevens, D. R.; Roberts, W. A.; Ojha, S. S.; Clarke, L. I.; Gorga, R. E. *Macromolecules* **2007**, *40* (4), 997−1003.
(56) Ojha, S. S.; Afshari, M.; Kotek, R.; Gorga, R. E. *J. Appl. Polym. Sci.* **2008**, *108* (1), 308−319.
(57) Ojha, S. S.; Stevens, D. R.; Hoffman, T. J.; Stano, K.; Klossner, R.; Scott, M. C.; Krause, W.; Clarke, L. I.; Gorga, R. E. *Biomacromolecules* **2008**, *9* (9), 2523−2529.
(58) Ojha, S. S.; Stevens, D. R.; Stano, K.; Hoffman, T.; Clarke, L. I.; Gorga, R. E. *Macromolecules* **2008**, *41* (7), 2509−2513.
(59) Ramaswamy, S.; Clarke, L. I.; Gorga, R. E. *Polymer* **2011**, *52* (14), 3183−3189.
(60) Weitz, R. T.; Harnau, L.; Rauschenbach, S.; Burghard, M.; Kern, K. *Nano Lett.* **2008**, *8* (4), 1187−1191.
(61) Higuera, F. J. *Phys. Rev. E* **2008**, *78* (1), 11.
(62) Angammana, C. J.; Jayaram, S. H. *IEEE Trans. Ind. Appl.* **2011**, *47* (3), 1109−1117.
(63) Angammana, C. J.; Jayaram, S. H. IEEE, Analysis of the Effects of Solution Conductivity on Electro-spinning Process and Fiber Morphology. In *2008 IEEE Industry Applications Society Annual Meeting*; IEEE: New York, 2008; Vols. *1*−*5*, pp 1890−1893.
(64) Stanger, J.; Tucker, N.; Kirwan, K.; Staiger, M. P. *Int. J. Mod. Phys. B* **2009**, *23* (6−7), 1956−1961.